Supplementary Material

Ruikun Zhang[1], Yan Yang[2], Liyuan Pan[1,3] *
[1]Beijing Institute of Technology, Beijing, China
[2]BDSI, Australian National University, Canberra, Australia
[3]Yangtze Delta Region Academy of Beijing Institute of Technology, Jiaxing, China
{ruikun.zhang, liyuan.pan}@bit.edu.cn, {yan.yang}@anu.edu.au

1. Overview

In this supplementary document, we provide additional experimental results that were omitted from the main paper due to space constraints. This document also includes implementation details and explanations of the evaluation metrics. We hope that these supplementary materials will facilitate a deeper understanding and more effective reproduction of our work by the research community.

2. Implementation Details

2.1. Pre-processing

During the preprocessing stage, previous methods typically cropped each spot image to 224×224 pixels based on the spot's center coordinates. Whole slide images (WSIs) typically have extremely high resolutions (e.g., one slide image in the breast cancer Visium HD dataset can reach a resolution of $25,550 \times 26,049$ pixels). Although our network is theoretically capable of processing the entire WSI to generate a full-resolution dense gene expression map, practical hardware constraints necessitate cropping the WSIs into smaller patches for inference and training.

To balance computational cost and model performance, we randomly crop patches of size $(1024 + 224) \times (1024 + 224)$ pixels directly from the whole slide tissue image. To reduce experimental noise, we adopt the smoothing strategy from [4], which averages each spot's gene expression values with those of its neighboring spots within the cropped region. The cropped patch is then center-cropped to 1024×1024 pixels to remove the extra margins. Spots falling outside this final crop are discarded.

For the remaining spots within each patch, we record their coordinates and sizes as supervision regions, and their corresponding gene expression values as supervision targets. These are used as ground truth to compute the sparse supervision loss during training. In each dataset, we select the top 250 most highly expressed genes following the criteria in [4]. The lists of the selected 250 genes for each dataset are shown in Figures 1 to 4. Gene expression values are standardized by first normalizing the total expression per spot, followed by log transformation. To reduce the preprocessing burden during training, all datasets are preprocessed and gene-filtered in advance using the aforementioned pipeline. Pyramidal feature maps are extracted from all image patches using the same pretrained image encoder and stored offline for efficient loading.

For the STnet [4] and Her2ST [1] datasets, we perform eight-fold cross-validation across all slide images. For the Visium HD datasets, we use all available samples, totaling over one million spots despite the limited number of slides. Specifically, for the breast cancer Visium HD dataset and the brain cancer Visium HD dataset, one slide is used for testing, while another is split $75/25$ for training and validation. In the results section, we report the mean and standard deviation of cross-validation results across all training datasets for all compared methods.

2.2. Evaluation Metrics

To assess the accuracy of spatial gene expression prediction, we follow several prior works [2, 3, 8, 11, 12] and adopt three widely used evaluation metrics: **mean squared error (MSE)**, **mean absolute error (MAE)**, and **Pearson correlation coefficient (PCC)**. These metrics capture both absolute differences and statistical correlation between predicted and ground truth gene expression values.

Mean Squared Error (MSE). The MSE measures the average of the squared differences between predicted and ground truth gene expression values. A lower MSE indicates better prediction accuracy.

$$\text{MSE} = \frac{1}{N} \sum_{n=1}^{N} (y_n - \hat{y}_n)^2 \tag{1}$$

where y_n is the ground truth gene expression value, $\hat{y}_n$ is the predicted value, and N is the number of spots.

*Corresponding author.

Mean Absolute Error (MAE). The MAE calculates the average absolute difference between the predicted and ground truth gene expression values, providing an interpretable metric of average prediction error. A lower MAE indicates better prediction accuracy.

$$\text{MAE} = \frac{1}{N}\sum_{n=1}^{N}|y_n - \hat{y}_n| \tag{2}$$

Pearson Correlation Coefficient (PCC). PCC measures the linear correlation between the predicted and ground truth gene expression values, ranging from -1 (perfect negative correlation) to 1 (perfect positive correlation). A higher PCC implies better alignment in expression patterns.

$$\text{PCC} = \frac{\sum_{n=1}^{N}(y_n - \bar{y})(\hat{y}_n - \bar{\hat{y}})}{\sqrt{\sum_{n=1}^{N}(y_n - \bar{y})^2}\sqrt{\sum_{n=1}^{N}(\hat{y}_n - \bar{\hat{y}})^2}} \tag{3}$$

where $\bar{y}$ and $\bar{\hat{y}}$ are the means of the ground truth and predicted values, respectively. To better quantify the distribution of gene prediction performance, we compute three statistics over the per-gene pearson correlation coefficients (PCC): PCC@F (first quartile), PCC@S (median), and PCC@M (mean), corresponding to the 25th percentile, 50th percentile, and average of PCC values across the selected 250 genes, respectively.

2.3. Baselines

Our method is compared against a range of existing approaches based on various network architectures, including 1) fine-tuning models pretrained on large scale datasets [4, 9, 11, 13]; 2) vision transformer based models [5, 7] and 3) graph based models [3, 6, 8, 10, 12, 14].

2.4. Experimental Setup

All experiments in this paper are implemented using PyTorch (version 2.0.1). All models are trained on an NVIDIA RTX A6000 GPU. To ensure reproducibility, a fixed random seed (233) is used across all implementations and reruns. Each training procedure is repeated five times, and the best-performing model is selected for each experiment. For baselines [2, 3, 8] assuming fixed spot sizes, we follow the standard practice [4, 7, 13] by central cropping to adapt them to different resolutions. In main paper's Table 1, 3, 4, and 6, baselines are trained and evaluated separately at each resolution and then averaged, whereas ours is trained with mixed-resolution supervision. Average GPU memory usage is 44 GB for training and 11 GB for inference.

2.5. Additional Qualitative Results

We provide additional qualitative results in Figures 5 and 6, to demonstrate the performance of our PixNet on a diverse range of samples.

References

[1] Alma Andersson, Ludvig Larsson, Linnea Stenbeck, Fredrik Salmén, Anna Ehinger, Sunny Wu, Ghamdan Al-Eryani, Daniel Roden, Alex Swarbrick, Åke Borg, et al. Spatial deconvolution of her2-positive breast tumors reveals novel intercellular relationships. *bioRxiv*, pages 2020–07, 2020. 1, 5

[2] Youngmin Chung, Ji Hun Ha, Kyeong Chan Im, and Joo Sang Lee. Accurate spatial gene expression prediction by integrating multi-resolution features. In *Proceedings of the IEEE/CVF Conference on Computer Vision and Pattern Recognition*, pages 11591–11600, 2024. 1, 2

[3] Aniruddha Ganguly, Debolina Chatterjee, Wentao Huang, Jie Zhang, Alisa Yurovsky, Travis Steele Johnson, and Chao Chen. Merge: Multi-faceted hierarchical graph-based gnn for gene expression prediction from whole slide histopathology images. In *Proceedings of the Computer Vision and Pattern Recognition Conference*, pages 15611–15620, 2025. 1, 2

[4] Bryan He, Ludvig Bergenstråhle, Linnea Stenbeck, Abubakar Abid, Alma Andersson, Ake Borg, Jonas Maaskola, Joakim Lundeberg, and James Zou. Integrating spatial gene expression and breast tumour morphology via deep learning. *Nature Biomedical Engineering*, 4:1–8, 2020. 1, 2, 5

[5] Masum Shah Junayed, Afsana Ahsan Jeny, Sheida Nabavi, and Ion Mandoiu. A fused transformer-based model for gene expression prediction using histopathology images. In *2024 IEEE International Conference on Bioinformatics and Biomedicine (BIBM)*, pages 4942–4949. IEEE, 2024. 2

[6] Bo Li, Yong Zhang, Qing Wang, Chengyang Zhang, Mengran Li, Guangyu Wang, and Qianqian Song. Gene expression prediction from histology images via hypergraph neural networks. *Briefings in Bioinformatics*, 25(6):bbae500, 2024. 2

[7] Minxing Pang, Kenong Su, and Mingyao Li. Leveraging information in spatial transcriptomics to predict super-resolution gene expression from histology images in tumors. *BioRxiv*, pages 2021–11, 2021. 2

[8] Mingcheng Qu, Yuncong Wu, Donglin Di, Anyang Su, Tonghua Su, Yang Song, and Lei Fan. Boundary-guided learning for gene expression prediction in spatial transcriptomics. In *2024 IEEE International Conference on Bioinformatics and Biomedicine (BIBM)*, pages 445–450. IEEE, 2024. 1, 2

[9] Ronald Xie, Kuan Pang, Sai Chung, Catia Perciani, Sonya MacParland, Bo Wang, and Gary Bader. Spatially resolved gene expression prediction from histology images via bimodal contrastive learning. *Advances in Neural Information Processing Systems*, 36:70626–70637, 2023. 2

[10] Shuailin Xue, Fangfang Zhu, Jinyu Chen, and Wenwen Min. Inferring single-cell resolution spatial gene expression via fusing spot-based spatial transcriptomics, location, and histology using gcn. *Briefings in Bioinformatics*, 26(1): bbae630, 2025. 2

[11] Yan Yang, Md Hossain, Eric Stone, and Shafin Rahman.

Selected 250 genes in the STNet dataset

RPS3, IGLL5, RPLP1, TFF3, RPS18, GAPDH, TMSB10, RPLP2, RPS14, RPL37A, RPS19, RPL28, KRT19, RPL8, RPL13, RPL19, ACTB, RPL36, RPL18A, RPL35, RPL18, RPS2, RPS12, RPS21, RACK1, RPL13A, CTSD, FTL, PFN1, MGP, RPS15, RPS11, RPS16, HLA-B, UBA52, NHERF1, RPS17, PSAP, RPLP0, SERF2, RPS27, RPS8, RPL27A, MUC1, RPS28, H2AJ, RPL10, CALR, RPS29, RPL38, RPL11, P4HB, RPS6, CST3, FTH1, RPS4X, SSR4, RPL30, ERBB2, APOE, AZGP1, RPL3, COX6C, HLA-C, FAU, RPS9, EEF2, B2M, RPS5, RPL12, ACTG1, RPS27A, RPL37, RPL23, HLA-A, RPL31, RPL29, RPL7A, IFI27, PABPC1, CD74, BEST1, RPL32, FASN, S100A9, GPX4, RPL15, RPL27, MZT2B, RPL23A, HSPB1, MALAT1, RPS24, COL1A1, C4B, KRT18, CFL1, CD81, ALDOA, RPL35A, SYNGR2, PPP1CA, HLA-E, TAGLN, RPL9, CD63, RPS3A, LGALS3BP, IGFBP2, BST2, TPT1, EDF1, RPS25, ATP6V0B, TAPBP, GRINA, XBP1, S100A11, NBEAL1, AEBP1, CCND1, OAZ1, RPL14, TAGLN2, FN1, PPDPF, BCAP31, IFITM3, PRDX1, BGN, GNAS, PTMA, UBC, MZT2A, SLC25A6, RPS20, HSP90AB1, RPS10, MYL6, CLDN3, ATP6AP1, PRDX2, RPL24, GNB2, RPL34, RPL4, LMNA, NDUFA13, HLA-DRA, SNHG25, TIMP1, H1-10, RPS23, COX8A, KRT8, LY6E, ENO1, GRN, PTPRF, RPL7, UBB, BSG, ELOB, COX6B1, TMSB4X, C1QA, PRSS8, RPL5, UQCR11, RPS7, A2M, RPS15A, VIM, S100A6, NDUFA11, PSMD3, EVL, APOC1, H3-3B, ATP5F1E, PLXNB2, MYL9, TUBA1B, CTSB, ISG15, FLNA, RPS13, NDUFB9, EIF4A1, POLR2L, CYBA, CRIP2, EEF1D, ATP1A1, ELF3, TUFM, SH3BGRL3, STARD10, C3, GUK1, ZNF90, C12orf57, TLE5, SEC61A1, SDC1, PLD3, SPDEF, ARHGDIA, IFI6, LAPTM5, RPL41, CLU, GNAI2, PFDN5, RPL39, SSR2, COX4I1, RHOC, JUP, EIF4G1, FXYD3, TSPO, UQCRQ, COL1A2, RPL10A, S100A8, SELENOW, TPI1, ATP5MC2, PTMS, IGFBP5, LGALS1, SPINT2, RPSA, GSTP1, CHCHD2, EIF5A, COX5B, ATG10, RPL6, EEF1A1, CAPNS1, LMAN2, UBE2M, SPARC, EIF3C, GAS5, TUBB, ACTN4, IGFBP4

Figure 1. List of the 250 genes selected in all experiments on the ST-Net dataset.

Selected 250 genes in the Her2ST dataset

IGKC, TMSB10, ERBB2, IGHG3, IGLC2, IGHA1, GAPDH, ACTB, IGLC3, IGHM, SERF2, PSMB3, PFN1, ACTG1, KRT19, RACK1, MUCL1, CISD3, APOE, MIEN1, SSR4, CALR, PSAP, CTSD, FTL, FTH1, TPT1, PTPRF, UBA52, P4HB, BEST1, HLA-B, FAU, SLC9A3R1, FN1, COL1A1, EEF2, IGHG4, CALML5, CD74, B2M, FASN, S100A9, MGP, CFL1, PSMD3, IGHG1, HLA-A, S100A6, MYL6, COL1A2, PHB, TAGLN2, HLA-E, HLA-C, KRT7, CD63, SYNGR2, STARD3, PABPC1, GPX4, GRB7, SLC25A6, AEBP1, GNAS, NDUFB9, EDF1, CRIP2, DDX5, OAZ1, EIF4G1, LMNA, GNB2, CST3, PCGF2, SDC1, S100A11, PRDX1, GRINA, ATP6V0B, TFF3, HLA-DRA, EEF1D, AZGP1, PPP1CA, FLNA, COL3A1, ATP5E, SPDEF, AP000769.1, ALDOA, PLXNB2, TAGLN, TUBA1B, APOC1, PRRC2A, LAPTM5, PTMS, KRT18, IFI27, PLD3, ADAM15, C1QA, AES, TSPO, MLLT6, TAPBP, SCAND1, ATP1A1, CD81, SEC61A1, CLDN3, PPDPF, S100A14, BGN, C3, MZT2B, S100A8, MDK, PFDN5, H2AFJ, SH3BGRL3, ENO1, XBP1, CYBA, COX6B1, TRAF4, CD24, PRSS8, MMP14, MUC1, VIM, MIDN, SPINT2, BST2, TIMP1, GUK1, ACTN4, CTSB, COX4I1, CCT3, HNRNPA2B1, SEPW1, LY6E, SCD, HSPB1, EIF4G2, BSG, ZYX, TUBB, LASP1, CD99, COL6A2, H1FX, RALY, UBE2M, SPARC, ATG10, HSP90AB1, ORMDL3, LMAN2, CHCHD2, COX7C, ARHGDIA, VMP1, UBC, IGFBP2, COPE, NUPR1, PERP, KRT81, PPP1R1B, LGALS3BP, SSR2, KIAA0100, MYL9, CIB1, IDH2, STARD10, LGALS1, COX6C, GRN, MAPKAPK2, GNAI2, KDELR1, COL18A1, UQCRQ, COX5B, ELOVL1, CHPF, CLDN4, C12orf57, LGALS3, HSP90AA1, JUP, A2M, NDUFB7, PGAP3, HSPA8, TCEB2, PEBP1, COPS9, ATP5G2, ATP6AP1, MYH9, LSM4, COX8A, UQCR11, ATP5B, DHCR24, PTBP1, EIF3B, NDUFA3, FKBP2, MMACHC, RABAC1, ISG15, PTMA, RRBP1, POSTN, C1QB, BCAP31, PSMB4, LAPTM4A, INTS1, FNBP1L, JTB, NBL1, HM13, SLC2A4RG, ROMO1, SERINC2, NDUFA11, RHOC, TXNIP, TYMP, NACA, HSP90B1, SNRPB, PFKL, VCP, ERGIC1, NUCKS1, PSMD8, CALM2, AP2S1, DBI, C4orf48, SDF4, TPI1

Figure 2. List of the 250 genes selected in all experiments on the Her2ST dataset.

Selected 250 genes in the breast cancer Visium HD dataset

IGKC, IGHG1, MT-CO3, MT-ATP6, CD24, MT-CO2, MT-ND4, COL1A1, MUCL1, MT-ND4L, MT-CYB, MT-ND2, CD74, APOD, FASN, COL1A2, COL3A1, CLU, TMSB4X, ERBB2, MT-ND3, SPARC, TMSB10, XBP1, MUC1, PIP, ACTB, MLPH, TFF1, KRT7, APOE, LTF, H3F3A, SLC39A6, S100A9, AZGP1, IGHG3, COX6C, MT-ND1, DDX5, EEF2, OAZ1, MAGED2, CD9, FN1, GLUL, IGHA1, MT-ND6, VIM, B2M, RHOB, DHRS2, ALDH3B2, NDUFC2, CIRBP, PSAP, CTSB, PRSS23, TSKU, CRYBG1, CST3, CSRP1, TPM1, SQSTM1, SERHL2, MARCKSL1, LMNA, GATA3, UCP2, MYL6, PFN1, CRIP1, CFB, EVL, TOB1, PDCD4, CFL1, CYB561, SLC9A3R1, RHOC, IFI6, CALCOCO2, STARD10, FTH1, HNRNPA2B1, LGALS1, LUM, CD44, COL6A2, TAPBP, PNMT, ACTG1, SPINT2, HSPB1, SULT1C3, ALCAM, DSP, APP, SYNGR2, SAT1, AEBP1, IGFBP4, KRT8, DCN, BST2, GRB7, MCL1, ANXA2, SCD, EPCAM, PRDX2, ZYX, HSPA8, PGAP3, NDUFS2, SERF2, UAP1, ZNF703, TIMP1, HSP90AB1, TFF3, SMARCD2, PSMD3, SERINC1, IGHD, ABCC11, S100A6, UBA52, SERPINH1, COL6A1, CD46, MAB21L4, COL6A3, AGR2, ELOVL5, CCDC47, ZFP36L1, CCNL2, IGFBP7, ADAR, MAT2A, ANKRD30A, MPV17L, STARD3, IFITM3, TAGLN, PSME1, CNN3, WFDC2, TSTD1, PSMC5, BGN, LY6E, MT-ND5, MGP, AHNAK, GPX4, UBE2Z, SLC7A2, PERP, TACSTD2, TAT, FTL, CCND1, IGLC1, SIAH2, F11R, NECTIN4, MMP11, RAB11FIP1, HSP90AA1, COL4A1, HNRNPF, CLDN4, CTSD, AKT1, CTSK, SSR2, CCNI, SNF8, TYMP, FABP7, RET, NDUFA4, TRAF4, CRABP2, CA12, CAPN2, CTTN, NUPR1, MARCKS, NPDC1, DHCR24, NME2, BCAM, TNFSF10, LMAN2, LITAF, ARRDC1, DNM2, FOS, GRINA, ELF3, CCN2, SLC38A1, ANKLE1, CD63, B4GALT1, COPG1, CD151, VMP1, BHLHE40, TMEM9, SELENOW, IER3, ATP6AP1, LAMP1, PEG10, LUC7L3, NME3, SCP2, SMIM14, GFRA1, CAPN1, S100A11, FAM214A, PPP4C, COMP, UBE2I, COL4A2, OS9, GSTK1, RAB13, CASC3, TBC1D9B, H1F0, BMPR1B, ELP2, PBX1, UFC1, ENAH, ERGIC3, MAPKAPK2, PTPRF, TANC2, CNDP2, PPDPF, CYB5A, CERS2, CTSZ

Figure 3. List of the 250 genes selected in all experiments on the breast cancer Visium HD dataset.

Selected 250 genes in the brain cancer Visium HD dataset

mt-Co2, mt-Co1, Camk2n1, mt-Atp6, mt-Co3, mt-Cytb, App, Snap25, Apoe, mt-Atp8, Ttr, Camk2a, Ncdn, Calm3, mt-Nd1, Uchl1, Selenow, Aldoc, Plp1, Olfm1, Itm2c, mt-Nd4l, Atp1b1, Tmsb4x, Cst3, Gpm6a, Mbp, Slc1a2, Eef1a2, Nrgn, Atp2a2, Ndrg4, Itm2b, mt-Nd5, Arf3, Tspan7, Dnm1, Map1b, Serinc1, Pcsk1n, Ptms, Pcp4, Snrpn, Cpe, Rtn4, Ndfip1, Snhg11, Vamp2, Tuba1a, mt-Nd4, Rtn1, Atp6v1b2, Ywhag, Ywhah, Stxbp1, Fth1, mt-Nd2, Aplp1, Atp1a3, Scn1b, Mdh1, Ptk2b, Rab6b, Stmn1, Syp, Ptprn, Sparcl1, Aldoa, Atp6v0a1, Mt3, Dynll2, Cck, Eno2, Atp2b1, Maged1, Sncb, Ppp3ca, Sez6l2, Sept5, Ppp1r9b, Map1a, Zwint, Syt1, Thy1, Clu, Syn1, Rtn3, Rab3a, Atp6v1a, Ckb, Basp1, Calm1, Ptprs, Atp6v1e1, Mobp, Rasgrp1, Gdi1, Mt1, Map1lc3a, Kif1b, Atp6ap1, Ptgds, Penk, Cadm4, Arpp21, Sptbn1, Kif1a, Tubb4a, Dlg4, Clstn1, Nptxr, Map2, Vsnl1, Rundc3a, Chn1, Cds2, Eif4a2, Uqcrc1, Slc17a7, Ahcyl1, Ppp3r1, Mlf2, Gnao1, Cyfip2, Atp1a2, Fbxl16, Gpm6b, Hpca, Slc22a17, Atp6v1c1, Ttc3, Gabarapl1, Sptan1, Tmem30a, Pfn2, Sept7, Cdk5r1, Atp6v0b, Mtch1, Atp2b2, Dctn1, Tcf25, Calm2, Ubqln2, Syt11, Ppp1r1b, Atp6ap2, Nisch, Ptov1, Cd81, Cadm2, Atp5o, Cadm3, Cap1, Atp6v0d1, Ppp2r1a, Gria2, Nap1l5, Nsf, Rabac1, Tmod2, Cx3cl1, Rab6a, Atp9a, Camkv, Map2k1, Lrp1, Ndrg2, Tspan3, Pld3, Ddx17, Spock2, Tmem181a, Atp1a1, Kalrn, Atp6v1g2, Hpcal4, Purb, Akt3, Prnp, Chchd2, Car2, Prkcb, Rhob, Nsg1, Map4, Uqcr11, Ttyh1, Stub1, Mapk1, Nsg2, Sptbn2, Tubb2a, Bin1, Cox7b, Atp6v0e2, Gabbr1, Akap5, Arf5, Camk2b, Zfp365, Akr1a1, Gnas, Iqsec1, Abr, Agap2, Atp6v1h, Sod2, Nptn, Tubb4b, Dclk1, Glul, Nefl, Nrxn2, Dpysl2, Sirpa, Tecr, Hspa8, Cplx1, Sult4a1, Stmn3, Tsc22d1, Ddn, Kif5c, Qk, Ywhae, Habp4, Sort1, Rasd2, Ldhb, Ntrk2, Lrrc4b, Kctd17, Lingo1, Rufy3, Ank2, Grin1, Tspyl4, Khdrbs3, Ngef, Gprasp1, Tagln3, Cfl1, Impact, Stx1b, Chchd10, Atp6v0c, Mllt11, Itfg1, Sept8

Figure 4. List of the 250 genes selected in all experiments on the brain cancer Visium HD dataset.

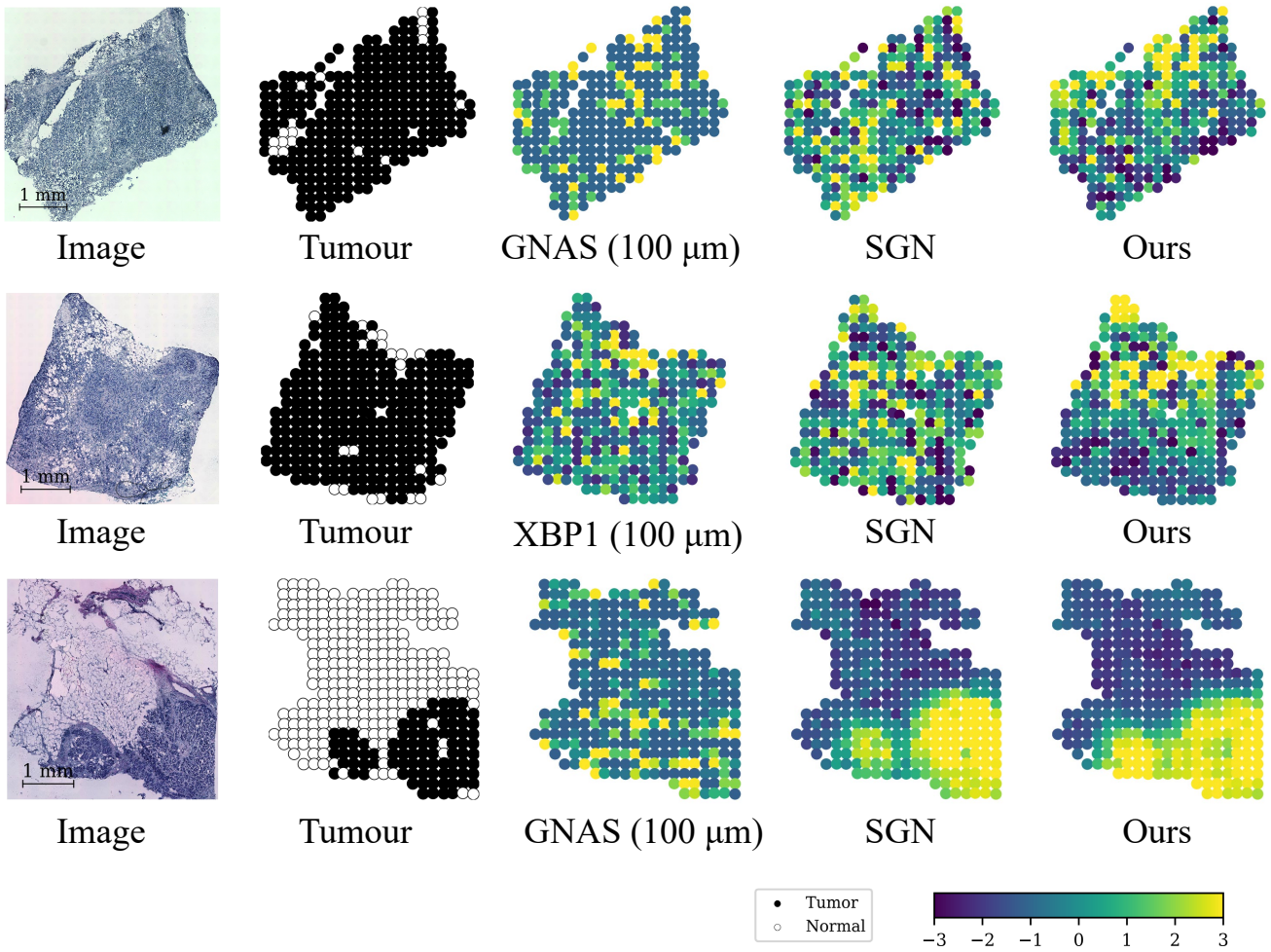

Figure 5. Examples of predicted gene expression on Stnet [4] and Her2ST [1] datasets. From left to right, we show the slide image, tumour annotation, ground truth gene expression, and predictions from various methods.

Exemplar guided deep neural network for spatial transcriptomics analysis of gene expression prediction. 2022. 1, 2

[12] Yan Yang, Md Zakir Hossain, Xuesong Li, Shafin Rahman, and Eric Stone. Spatial transcriptomics analysis of zero-shot gene expression prediction. In *International Conference on Medical Image Computing and Computer-Assisted Intervention*, pages 492–502. Springer, 2024. 1, 2

[13] Yan Yang, Md Zakir Hossain, Eric Stone, and Shafin Rahman. Spatial transcriptomics analysis of gene expression prediction using exemplar guided graph neural network. *Pattern Recognition*, 145:109966, 2024. 2

[14] Daiwei Zhang, Amelia Schroeder, Hanying Yan, Haochen Yang, Jian Hu, Michelle YY Lee, Kyung S Cho, Katalin Susztak, George X Xu, Michael D Feldman, et al. Inferring super-resolution tissue architecture by integrating spatial transcriptomics with histology. *Nature biotechnology*, 42(9):1372–1377, 2024. 2

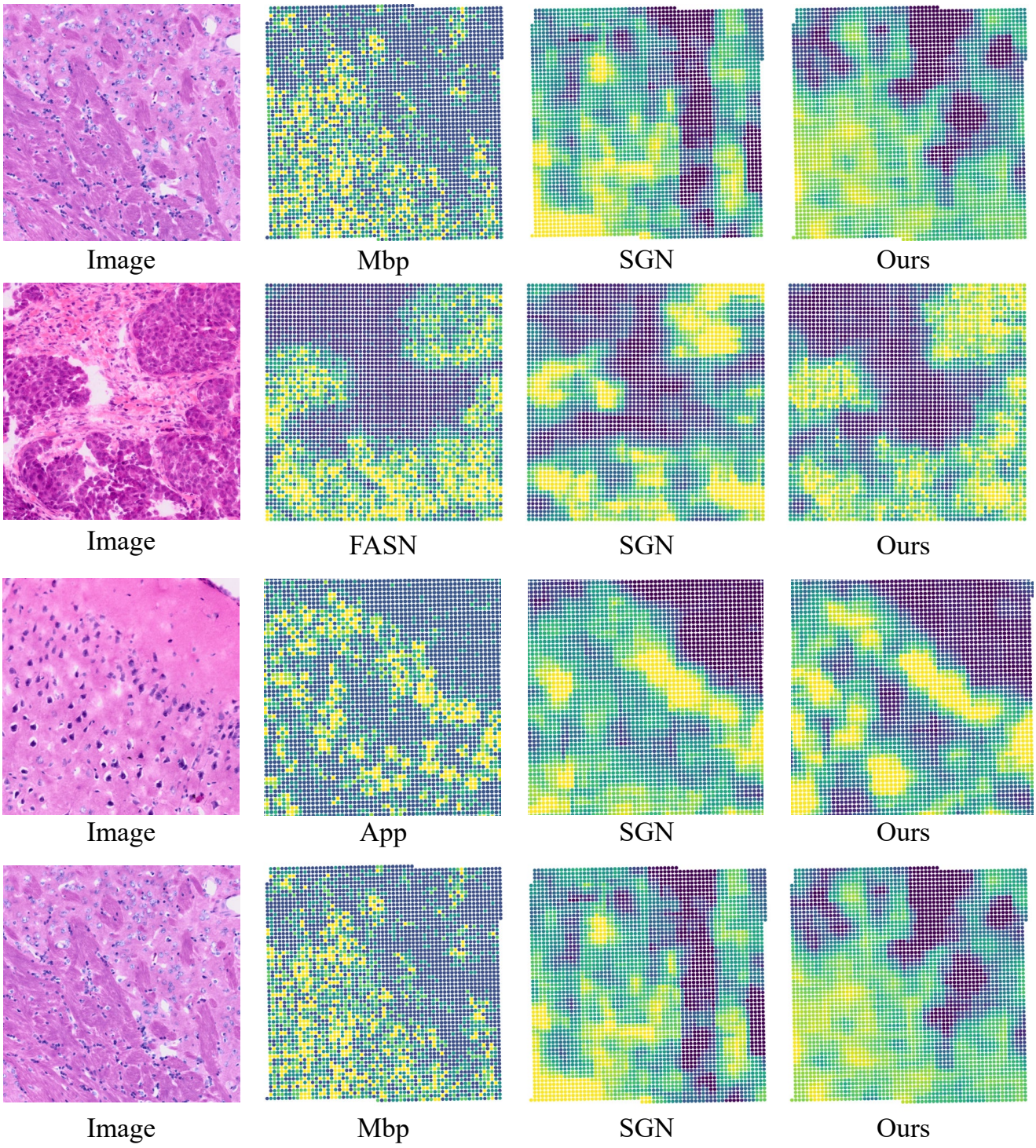

Figure 6. Examples of predicted gene expression on Visium HD datasets. From left to right, we show the slide image, tumour annotation, ground truth gene expression, and predictions from various methods.